Effect of welding on the tensile behavior of high strength steel T-stub joints - Part 1: Experimental and analytical study

Zhao, Ming Shan; Chen, C.; Chiew, S. P.

2015

Zhao, M. S., Chen, C., & Chiew, S. P. (2015). Effect of welding on the tensile behavior of high strength steel T-stub joints - Part 1: Experimental and analytical study. 11th International Conference on Advances in Steel and Concrete Composite Structures.

https://hdl.handle.net/10356/80612

11th International Conference on
Advances in Steel and Concrete Composite Structures
Tsinghua University, Beijing, China, December 3-5, 2015

EFFECT OF WELDING ON THE TENSILE BEHAVIOR OF HIGH STRENGTH STEEL T-STUB JOINTS - PART I: EXPERIMENTAL AND ANALYTICAL STUDY

M.S. Zhao[a], C. Chen[b]& S.P. Chiew[c]

[a] Research fellow, [b] Graduate Student, School of Civil Engineering, Nanyang Technological University, Singapore
E-mails: mszhao@ntu.edu.sg, cchen013@ntu.edu.sg

[c] Professor of Civil Engineering, Singapore Institute of Technology, Singapore
E-mail: SingPing.Chiew@SingaporeTech.edu.sg

Keywords:
Effect; Welding; Tensile Behavior; High Strength Steel; T-stub Joints

A B S T R A C T

In this study, experiments were conducted to study the tensile behavior of 10 T-stub joints made of emerging structural steel including reheated, high strength steel S690, normal strength steel S440 and S385. The results are further validated against the developed yield line approach and the design load carrying capacity equations provided by EC3. It is found that the behavior of the T-stub joints made of S385 and S440 agree well with the analytical approach and the load carrying capacities can be conservatively predicted by EC3. However, although the S690 shows superior load carrying capacities than the S440 and S385, the results are obviously lower than the anticipation of the analytical approach and the prediction by EC3. In addition, the ductility of the S690 specimens is much worse than that of the S440 and S385 specimens, which may result in more brittle failure modes.

1 INTRODUCTION

With the development of design and construction technology, the evolution of steels for structural usage never stops. The replacement of traditional normal strength steels by emerging high strength and high performance steels is on the way. Due to higher strength to weight ratio, saving in total materials and convenience in construction, higher construction productivity can be achieved by replacing normal strength steels with high strength steels. However, the differences between the emerging high strength steels and the traditional normal strength steels are much more than just strength.

Strength of steel is usually enhanced by either adding alloying elements or going through heat treatments/work hardening. Different from high alloy steels, heat treated steels offer better performance in yield and tensile strength without sacrificing much weldability. Therefore, such kinds of steel have occupied most of the high strength structural steel market. One major issue against the popularization of HSS is that the quenching and tempering process improves the strength at the expense of ductility through complicated heat treatments. Massive researches have demonstrated that it is not possible for QT steels to achieve good deformation capacity (Bjorhovde 2004; Girão Coelho and Bijlaard 2007; Uy 2008) and they are more susceptible to heat (Chen and Young 2006; Qiang, Bijlaard et al. 2012) than mild steels, as inherited from the heat-treatment hardened microstructures (Bhadeshia and Honeycombe 2006). As a result, it is foreseeable that welding may be an issue stopping HSS from becoming popular. Nevertheless, despite the large number of reports claiming the existence of welding issues (high residual stress level and HAZ property alternation) in HSS, few works regarding the effects of these issues on the performance of HSS structures can be found in literature, let alone the recommendations and cautions given for designing or evaluating the performance of HSS structures.

In this paper, the tensile performance of T-stub joints made of two types of emerging structural steels, i.e. Reheated, Quenched and Tempered (RQT) Steels in grade S690 and Thermal-Mechanical Controlled Processed (TMCP) steels in grade S440 and S385 are presented. 10 specimens in the same configuration with different materials and thicknesses are fabricated and tested. A non-linear analytical approach based on the yield line model (Girão Coelho, Bijlaard et al. 2004;

Al-Khatab and Bouchaïr 2007; Fernandez-Ceniceros, Sanz-Garcia et al. 2015) is developed to predict the load-displacement relationships of these joints. By comparing the test results, yield line model results and the design equations given in EN 1993-1-8 (BSI 2005), the performance of these joints are evaluated.

2 EXPERIMETAL STUDY

2.1 *Material*

Three grades of steels are examined in this study: TMCP steel plates in grades S385 (16mm) and S440 (22mm) and RQT in grade S690 (8mm, 12mm and 16mm). Both types of materials are emerging for the structural usage in contrast to the traditional NSS S355 or mild steels S235 and S275. The mechanical properties of the studied materials obtained by standard coupon tensile test are presented in Table 1, in comparison with the corresponding standards including EN 10025-4 (BSI 2004) and EN 10025-6 (BSI 2004) for TMCP and RQT products, respectively. From Table 1, two distinct features of RQT-S690 can be read: First, This material has superior strengths compared to traditional steels. The actual yield strength of RQT-S690 is more than twice of the nominal yield strength of S355. Second, RQT-S690 is very brittle compared to traditional NSS or the two TMCP steels in this study. For TMCP, it can also be seen from Table 1 that the TMCP-S385 literally fulfilled the mechanical property specifications of S420M/ML and the TMCP-S440 fulfilled those of S460M/ML.

Table 1. Mechanical properties of RQT-S690, TMCP-S385 and TMCP-S440

Grade	fy(MPa)	fu(MPa)	E(GPa)	δ(%)
RQT-S690	745.2.0	837.8	208.9	14.5
S690Q/QL	690	770-940	-	14
TMCP-S440	527.3	601.3	206.9	29.2
S460M/ML	440	540-720	-	17
TMCP-S385	443.3	568.0	208.4	37.8
S420M/ML	420	520-680	-	19

2.2 *Specimen and Test Set-up*

10 T-joints were fabricated and tested in this study. They were of the same configuration but different thicknesses and materials. Each specimen is fabricated by joining two identical sheets with dimensions of 440×150×t mm, where t is the thickness. The joints are designed as complete joint penetration butt weld according to the AWS structural steel welding code (AWS 2008). To finish the weld work, the SMAW method was employed. Compared to the other common welding methods, SMAW is more friendly to martensite-based high strength steel due to the low heat input (Mohandas, Madhusudan Reddy et al. 1999) which may less affect the HAZ.

The tensile tests for the T-stub joints were carried out in a servo-hydraulic universal test machine that has a maximum loading capacity of 2000KN. To fix the specimen into the test machine, support joints made of S355 steel plates with thickness of 50mm were fabricated. The configurations of the support joints are the same as those of the test joints. The specimens are fixed into the support joints by 6 high strength hexagon bolts in grade 10.9HR, M24. The full set-up is shown in Figure 1.

Figure 1. The tensile test setup

2.3 *Test Results*

2.3.1 *General descriptions*

Figures 2 and 3 present the test results in terms of load-displacement curves of the TMCP and RQT steel T-stub joints, respectively. Despite that the specimens may fail in different modes, the curves are of the same pattern. In general, three stages in the load-displacement curves can be distinguished: (1) the elastic stage, (2) plastic hinge development stage and (3) the failure stag. In the elastic stage, stiffness and the elastic modulus govern the behaviors of the joints until general yielding takes place. Within this stage, the load increases rapidly with a high load / displacement ratio, which is dependent on the stiffness of the joint, more specifically, the angle and thickness. When the specimens are further loaded, plastic deformation would appear and obvious plastic hinges could be seen. The positions of the plastic hinges are almost fixed: two at near the weld toes and the other two near the bolt hole, as shown in Figure 4. In this stage, the deformation grows wildly but the carried load increases slowly. It is worth noting that the curves of the same angle group are generally parallel to each other. If the loads are further increased, stronger hardening effects than those in the plastic hinge development stage occur and the parallel relationship in the Load-displacement curves of each angel group disappear. In a short loading time, final failure appeared as either weld toe through thickness fracture or bolt hole necking failure.

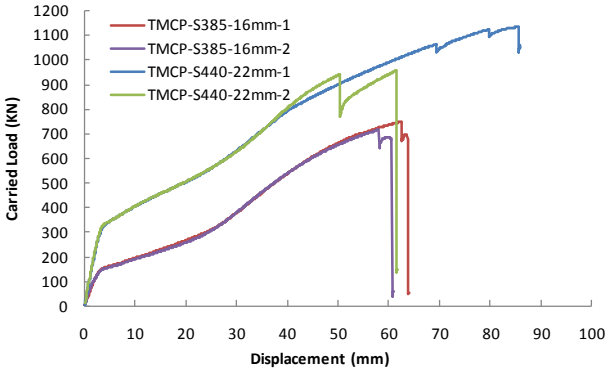

Figure 2. Load-Displacement of the TMCP-S385 and S440 T-stub joints

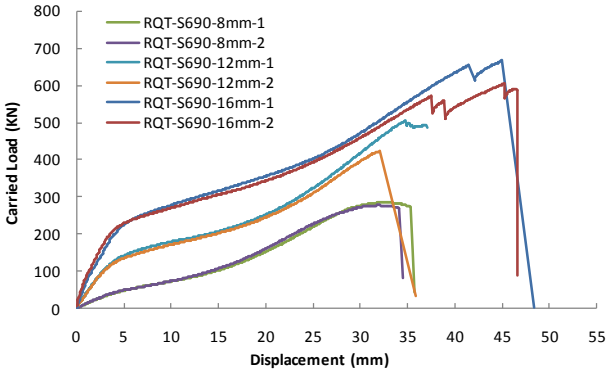

Figure 3. Load-Displacement of the RQT-S690 T-stub joints

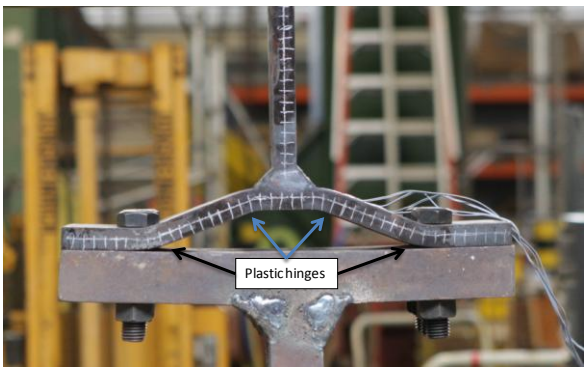

Figure 4. Plastic hinge phenomena

2.3.2 *Stiffness of the elastic stage*

For design purpose, the ultimate load carrying capacity or the behavior of the joints under the elastic stage is of the most importance. From Figures 2 and 3, it can bee seen that not only the stiffness but also the deformation limit of the elastic stage vary according to the configuration and material of the specimens. To quantitatively evaluate these two parameters, the yield line theory is introduced. The elastic stage and plastic hinge development stage of the curves are taken out and simplified into straight line model, as shown in Figure 5. The turning point is defined as the plastic resistance, which is widely accepted as the load carrying capacity before large deformation appears (Al-Khatab and Boucha ŕ 2007). Based on the simplified load-displacement model, the global stiffness of the studied T-stub joints under the elastic stages is defined as:

$$E_G = \frac{F_L}{D} \qquad \text{(Eqn. 1)}$$

, where E_G is the global stiffness; F_L is the load at certain level of elastic displacement d.

The calculated stiffness for all the tested joints is shown in Figure 6. It can be seen from Figure 6 that the test results are repeatable and stable. The maximum differences between the specimens in the same configuration occurred at the RQT-S690-8 and 16mm and are only 3.2%. The stiffness in terms of carried load (KN) per displacement (mm) increases rapidly with the thickness of the specimens. The stiffness of the 16mm RQT specimens is about 5.3 times of that of the 8mm RQT specimens, while the stiffness of the TMCP-22mm is slightly less than 2 times of that of the TMCP-16mm. Besides, although the RQT-S690-16mm and the TMCP-S385-16mm had exactly the same configuration, the RQT-S690-16mm specimens show slightly higher stiffness. From Figure 6, it can be seen that the stiffness-thickness relationship is generally linear. The equation of the trend line is obtained and expressed as:

$$y=6.520x-40.98 \qquad \text{(Eqn. 2)}$$

It can be seen from Figure 6 that the trend line equation agreed well with the test results, except for the TMCP-S385-16mm. For the rest, the maximum difference is only 4.0%.

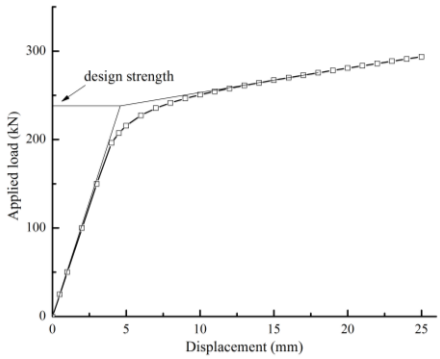

Figure 5. Simplified elastic-plastic load-displacement curve

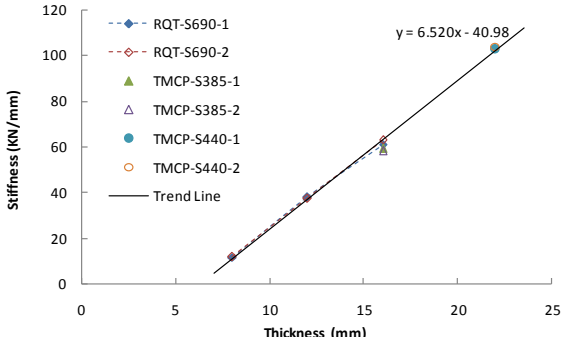

Figure 6. Stiffness of the elastic stage

3 ANALYTICAL APPROACH

Various analytical approaches for the load-displacement relationships of the T-stub joints have been developed in different complexity. From plastic analysis, Zoetemeijer (Zoetemeijer 1974) derived the failure loads of the T-stub joints under all three failure modes. Based on his models, many researchers have further developed the yield line theory to solve the initial stiffness and the plastic resistance with higher precision (Girão Coelho, Bijlaard et al. 2004; Al-Khatab and Bouchaïr 2007; Yu, Burgess et al. 2009). In this paper, a yield line model is established for the T-stub joints made of RQT-S690 and TMCP-S385 and S440. Similarly, this model focuses on the initial stiffness and plastic resistance at relatively small deformation stage.

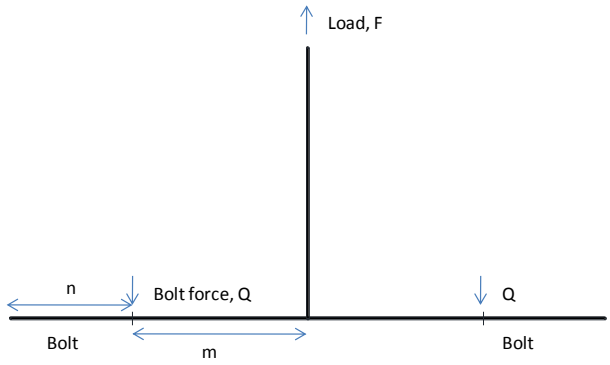

Figure 7. T-stub joints before deformation

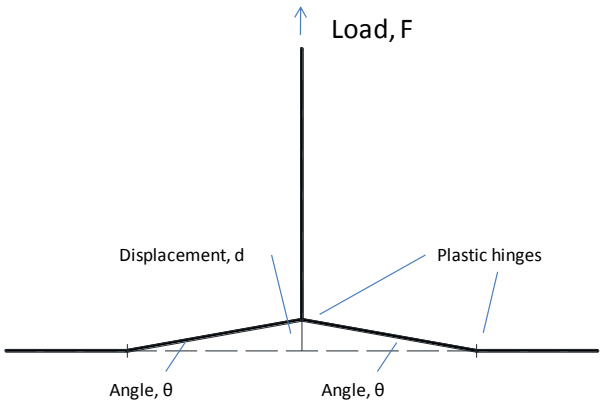

Figure 8. T-stub joints after deformation

The geometrical models of the T-stub before and after deformation are shown in Figures 7 and 8. Assuming the prying force at both ends of the chord plate to be negligible, the work that load F has done is fully transferred to the strain energy of the plastic hinges according to the virtual work principle:

$$Fd = W_{ph} = 4 \qquad \text{(Eqn. 3)}$$

where F is reaction force at displacement d, M is plastic hinge rotation capacity and θ is the angle at deformation d, as shown in Figure 8.
By simple geometry analysis,

$$d = m\tan\theta = m\theta. \qquad \text{(Eqn. 4)}$$

Therefore, Eqn. 3 can be simplified as

$$F = 4\,{}^{M}/_{m} \qquad \text{(Eqn. 5)}$$

Based on the stress-strain curves of the three materials obtained by standard coupon tensile test, the simplified two-stage true elastic-plastic stress-stain curves are derived, as shown in Figure 9. The definitions of the symbols of the stress-strain curves are shown in Figure 9. For the TMCP materials, E_p=0. Depending on the maximum strain ε_m (located at the surface), there are two possible patterns of stress/strain distribution over the cross section of the plastic hinge, as shown in Figure 10b. When the cross section is not yielded, i.e. $\varepsilon_m \le \varepsilon_y$,

$$\sigma = E\frac{x}{t/2}\varepsilon_m \qquad \text{(Eqn. 6)}$$

When $\varepsilon_m > \varepsilon_y$,

$$\sigma = \begin{cases} E\frac{x}{t/2}\varepsilon_m & x < \frac{\varepsilon_y}{\varepsilon_m}\frac{t}{2} \\ f_y + E_p\left[\frac{x}{t/2}\varepsilon_m - \varepsilon_y\right] & x > \frac{\varepsilon_y}{\varepsilon_m}\frac{t}{2} \end{cases} \qquad \text{(Eqn. 7)}$$

The moment at the plastic hinge can be calculated from integration of the stresses over the cross-section:

$$\text{For } \varepsilon_m \le \varepsilon_y,\ M = 2l_{eff}\int_0^{t/2}\sigma x dx = 2l_{eff}\left(\frac{t}{2}\right)^2\left(\frac{1}{3}E\varepsilon_m\right) \qquad \text{(Eqn. 8)}$$

$$\text{For } \varepsilon_m > \varepsilon_y,\ M = 2l_{eff}\int_0^{t/2}\sigma x dx = 2l_{eff}\left(\frac{t}{2}\right)^2\left[\frac{1}{3}E\varepsilon_m + \frac{1}{2}(E - E_p)\varepsilon_y - \frac{1}{6}(E - E_p)\frac{\varepsilon_y^3}{\varepsilon_m^2}\right] \qquad \text{(Eqn. 9)}$$

Assume the curvature of the cross section is

$$\gamma = \frac{\varepsilon_m}{t/2}$$

and the length of the plastic hinge is

$$k\left(\frac{t}{2}\right)$$

at small displacements (Yu, Burgess et al. 2009), the rotation of the plastic hinge can be calculated as:

$$\theta = \int_0^{k\frac{t}{2}}\frac{\varepsilon_m}{t/2} = k\varepsilon_m \qquad \text{(Eqn. 10)}$$

With Eqn. 4, Eqn. 9 can be rewritten as:

$$\varepsilon_m = \frac{d}{km} \qquad \text{(Eqn. 11)}$$

Thus, Eqn. 8 and 9 can be expressed as:

$$\text{For } d \le km\varepsilon_y,\ M = 2l_{eff}\left(\frac{t}{2}\right)^2\left(\frac{1}{3}E\frac{d}{km}\right) \qquad \text{(Eqn. 12)}$$

$$\text{For } d > km\varepsilon_y,\ M = 2l_{eff}\left(\frac{t}{2}\right)^2\left[\frac{1}{3}E\frac{d}{km} + \frac{1}{2}(E - E_p)\varepsilon_y - \frac{1}{6}(km)^2(E - E_p)\frac{\varepsilon_y^3}{d^2}\right] \qquad \text{(Eqn. 13)}$$

Substituting Eqn. 12 and 13 into Eqn. 5, the solution of F

can be expressed as:

$$F = \begin{cases} \frac{2l_{eff}}{m} t^2 \left(\frac{1}{3} E \frac{d}{km}\right), & d \le km\varepsilon_y \\ \frac{2l_{eff}}{m} t^2 \left[\frac{1}{3} E \frac{d}{km} + \frac{1}{2}(E - E_p)\varepsilon_y - \frac{1}{6}(km)^2 (E - E_p)\frac{\varepsilon_y^3}{d^2}\right], & d > km\varepsilon_y \end{cases} \quad \text{(Eqn. 14)}$$

Thus, the carried load F is expressed as a function of the displacement d.

It should be noted that at a state that the cross section is fully plastic instead of partially plastic (Figure 10b), M can be expressed as

$$M = l_{eff}(\frac{t}{2})^2 f_y$$

and similarly F can be expressed as

$$F = \frac{4 l_{eff} (t/2)^2 f_y}{m} \quad \text{(Eqn. 15)}$$

, which is the equation adopted by EC3 as the load carrying capacity (BSI 2005).

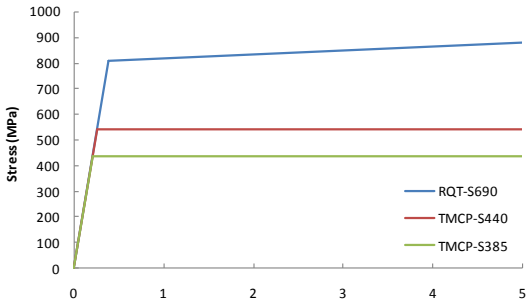

Figure 9. Simplified stress-strain curves for the analytical approach

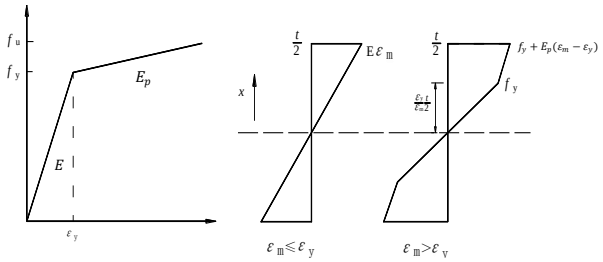

(a) Stress-strain model (b) Stress distributions in the section of the plastic hinges

Figure 10. Behavior of the plastic hinge

The parameter k in Eqn. 14 is dependent on the geometry of the specimen and material used to fabricate the joints. By checking the stiffness of the elastic stage, the values of k for RQT-S690, TMCP-S440 and TMCP-S385 are obtained: 8, 9.8 and 10.6, respectively. Note that this k is decreasing with the increasing thickness - showing that the difficulty of bending the material is increasing. Load-displacement relationships obtained by expressing Eqn. 14 for RQT and TMCP T-stub joints are shown in Figures 11 and 12. It can be seen from Figures 11 and 12 that the yield line approach (abbreviated as YL) agrees well with the TMCP test results but are generally higher than the RQTS-690 test curves since the end of the elastic stage.

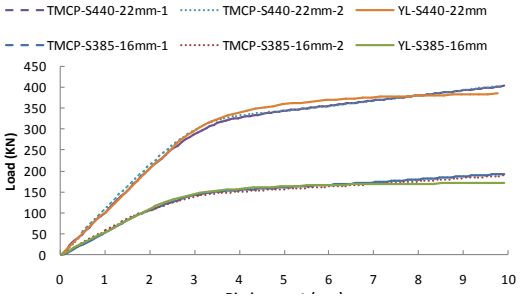

Figure 11. Comparison of the load-displacement curves of TMCP

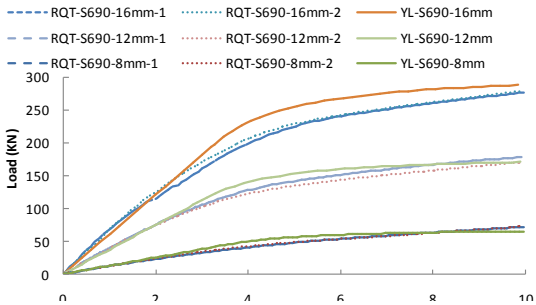

Figure 12. Comparison of the load-displacement curves of RQT-S690

4 PLASTIC RESISTANCE

In EC3, there are three failure modes for typical T-stub joints, i.e. 1, complete yielding of the flange, 2, bolt failure with yielding of the flange and 3, bolt failure (BSI 2005). In this study, all the specimens are failed in failure mode 1 and only slight plastic deformation was found in the bolts for TMCP-S440-22mm. The EN 1993-1-8 (BSI 2005) gives two methods based on yield line analysis to predict the load carrying capacity of the T-stub joints failed in complete yielding of the flange:

$$\text{Method 1: } F = \frac{4M_{pl,1,Rd}}{m} \quad \text{(Eqn. 16)}$$

$$\text{Method 2: } F = \frac{(8n - 2e_w)M_{pl,1,Rd}}{2mn - e_w(m+n)} \quad \text{(Eqn. 17)}$$

, where $M_{pl,1,Rd} = l_{eff}(t/2)^2 f_y$ is the design moment resistance of the section, leff, m, n are geometrical parameters of the T-stub joints, as shown in Figure 7; ew is 1/4 of the washer diameter or the width across points of the bolt head of nut, as relevant. In method 2, the force applied to the T-stub flange b a bolt is assumed to be uniformly distributed under the washer, the bolt head or the nut, instead of concentrated at the center line of the bolt. This assumption leads to higher value but is more

realistic, since the distance between the center lines of the weld toe plastic hinge and bolt area plastic hinge is smaller than m especially at the beginning of the plastic hinge development stage, as shown in Figure 4.

The load carrying capacities of the studied T-stub joints obtained by the yield line method and EC3 equations are shown in Figure 13. From Figure 13, it can be seen that the load carrying capacity of the RQT specimens are superiors compared to the TMCP specimens. The average load carrying capacity of the RQT-S690-16mm is about 91.3% more than that of the TMCP-S385-16mm. However, the test results of the RQT-S690 specimens are generally below anticipation compared to the EC3 equations. The load carrying capacity of the RQT-S690-8mm is much lower than both Eqns. 16 and 17, and the RQT-S690-12mm and 16mm are only slightly higher than Eqn. 16 and lower than Eqn. 17. On the contrary, the test results of the TMCP specimens are about 20% higher than the Eqn. 16 and at least 11.4% higher than the Eqn. 17. Accordingly, it seems that the load carrying capacity equations in EC3 are conservative for the TMCP-S385 and S440 but not conservative for the RQT-S690.

The plastic resistances of the YL models are obtained by using the approach shown in Figure 5. The results in percentage compared to the results calculated by using Eqn. 3 are shown in Table 6 and Figure 14. From Table 6 and Figure 14, it can be seen that the yield line approach can well predict the plastic resistances of the TMCP joints. The results of the yield line approach are about 30% higher than those of the Eqn. 3 and only 10% higher than the average value of the test results. However, for RQT-S690, the test results do not meet the anticipation by the yield line model and EC3 equations. As shown in Figure 14, the lines of the Eqns. 3 and 4 and the yield line models are generally parallel. The test results of the TMCP specimens fall in the gap between the yield line model and Eqn. 4, while those of the RQT-S690 are not higher than Eqn. 4, especially for the RQT-S690-8mm specimens. Further analysis of the differences between the yield line model and the average test results (Column 8, Table 6) show that test results of RQT-S690 are 20.9 to 33.3% lower than the yield line model and this difference decrease with the thickness.

Since the load carrying capacity is almost fully dependent on the moment resistances of the plastic hinges, it is highly susceptible that the problem comes from the properties of the plastic hinge at the weld toe. According to the material property study of HSS by Chiew (Chiew, Zhao et al. 2014), the mechanical properties of HSS may deteriorate at elevated temperatures and after exposure to high temperatures. Since the welding would induce localized, large and transient heat input into the fusion zone, the mechanical properties of HSS may be severely changed in the heat affected zone. As a result, the moment resistance of the plastic hinge at the weld toe is different form that at the bolt area and Eqn. 7 can no longer assume $F = 4\,M/m$. On the other hand, the heat affected zone is only a small area in the base metal adjacent to the fusion zone, the effect of the heat affected zone on the load carrying capacity may decrease with the increasing thickness as discussed previously.

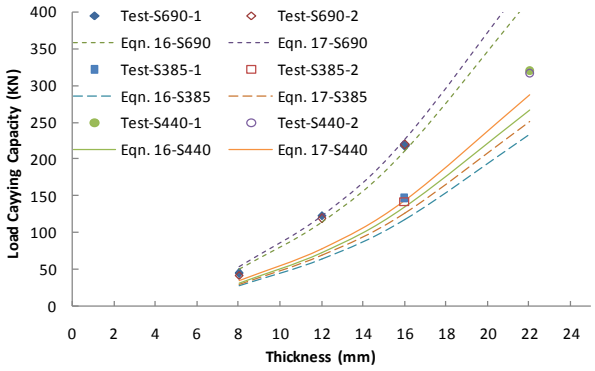

Figure 13. Load Carrying Capacities

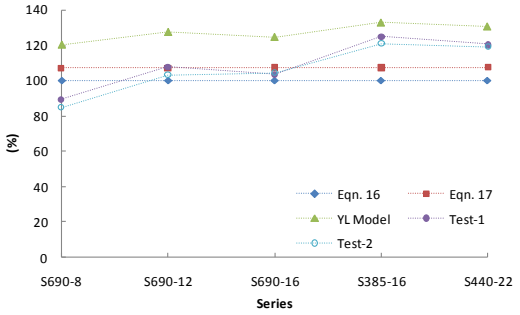

Figure 14. Plastic resistances of the yield line models

5 CONCLUSIONS

Experiments were conducted to study the tensile behavior of 10 T-stub joints made of emerging structural steels including reheated, high strength steel S690, normal strength steel S440 and S385. The results are further validated against the developed yield line approach and the design load carrying capacity equations provided by EC3. The results show that the behavior of the T-stub joints made of TMCP-S385 and S440 agree well with the analytical approach and the load carrying capacities can be conservatively predicted by EC3. However, the T-stub joints made of RQT-S690 behave differently from the TMCP specimens and the analytical approach. The stiffness at the elastic stage and plastic hinge development stage is similar to the TMCP specimens, but the load carrying capacities are below anticipation of the analytical approach and the prediction of EC3. The test results of the TMCP specimens are between the yield line model and EC3, while those of the RQT-S690 are not higher than the upper bound of EC3. Further discussion deducts that the problem may come from the compromised properties of the plastic hinges at the weld

toe, which is highly possible to be affected by welding heat input.

6 ACKNOWLEDGEMENT

This research is supported by the Singapore Ministry of National Development (MND) Research Fund on Sustainable Urban Living (Grant No. SUL2013-4). Any opinions, findings and conclusions expressed in this paper are those of the writers and do not necessarily reflect the view of MND, Singapore.

7 REFERENCES

- Al-Khatab, Z. and A. Bouchaïr (2007). "Analysis of a bolted T-stub strengthened by backing-plates with regard to Eurocode 3." Journal of Constructional Steel Research 63(12): 1603-1615.
- AWS (2008). Structural Welding Code. steel. Miami, American National Standards Institue.
- Bhadeshia, H. K. D. H. and R. W. K. Honeycombe (2006). Steels: microstructure and properties. Oxford, United Kingdom, Elsevier Science & Technology.
- Bjorhovde, R. (2004). "Development and use of high performance steel." Journal of Constructional Steel Research 60(3–5): 393-400.
- BSI (2004). Hot Rolled Products of Structural Steels: Part 4 Technical Delivery Conditions for Thermalmechanical Rolled Weldable Fine Grain Structural Steels, BS EN 10025-4. London, British Standards Institution.
- BSI (2004). hot rolled products of structural steels: part 6 technical delivery conditions for flat products of high yield strength structural steels in the quenched and tempered condition, BS EN 10025-6. London, British Standards Institution.
- BSI (2005). Eurocode 3: design of steel structures: part 1-8 design of joints, BS EN 1993-1-8. London, British Standard Institution.
- Chen, J. and B. Young (2006). "Behavior of High strength structural steel at elevated temperatures." Journal of structural eninggering: P1948-1954.
- Chiew, S. P., M. S. Zhao, et al. (2014). "Mechanical properties of heat-treated high strength steel under fire/post-fire conditions." Journal of Constructional Steel Research 98(0): 12-19.
- Fernandez-Ceniceros, J., A. Sanz-Garcia, et al. (2015). "A numerical-informational approach for characterising the ductile behaviour of the T-stub component. Part 1: Refined finite element model and test validation." Engineering Structures 82: 236-248.
- Girão Coelho, A. M. and F. S. K. Bijlaard (2007). "Experimental behaviour of high strength steel end-plate connections." Journal of Constructional Steel Research 63(9): 1228-1240.
- Girão Coelho, A. M., F. S. K. Bijlaard, et al. (2004). "Experimental assessment of the behaviour of bolted T-stub connections made up of welded plates." Journal of Constructional Steel Research 60(2): 269-311.
- Mohandas, T., G. Madhusudan Reddy, et al. (1999). "Heat-affected zone softening in high-strength low-alloy steels." Journal of Materials Processing Technology 88(1–3): 284-294.
- Qiang, X., F. Bijlaard, et al. (2012). "Dependence of mechanical properties of high strength steel S690 on elevated temperatures." Construction and Building Materials 30(0): 73-79.
- Uy, B. (2008). "Stability and ductility of high performance steel sections with concrete infill." Journal of Constructional Steel Research 64(7–8): 748-754.
- Yu, H., I. W. Burgess, et al. (2009). "Development of a yield-line model for endplate connections in fire." Journal of Constructional Steel Research 65(6): 1279-1289.
- Zoetemeijer, P. (1974). "A design method for the tension side of statically loaded, bolted beam-to-column connections." HERON 20(1).